Supporting Information for

Phosphorescent Sensor for Biological Mobile Zinc

Youngmin You,[a,b]* Sumin Lee,[b] Taehee Kim,[c] Kei Ohkubo,[d] Weon-Sik Chae,[e] Shunichi Fukuzumi,[b,d] Gil-Ja Jhon,[c] Wonwoo Nam,[b]* and Stephen J. Lippard[a]*

[a]Department of Chemistry, Massachusetts Institute of Technology, Cambridge, Massachusetts 02139,

[b]Department of Bioinspired Science, Ewha Womans University, Seoul 120-750, Korea,

[c]Department of Chemistry and Nano Science, Ewha Womans University,

[d]Department of Material and Life Science, Graduate School of Engineering, Osaka University, ALCA, Japan Science and Technology Agency (JST), Suita, Osaka 565-0871, Japan, and

[e]Korea Basic Science Institute, Gangneung center, Gangneung, Ganwondo 210-702, Korea

CONTENTS

Experimental Details

Materials and Synthesis. Commercially available chemicals were used as received. All glassware and magnetic stirring bars were thoroughly dried in a convection oven. Reactions were monitored using thin layer chromatography (TLC). Commercial TLC plates (silica gel 254, Merck Co.) were developed and the spots were visualized under UV light at 254 or 365 nm, or they were stained with *p*-anisaldehyde. Silica gel column chromatography was performed with silica gel 60 G (particle size 5 – 40 μm, Merck Co.). Multinuclear NMR spectra were collected with a Bruker AVANCE-400 NMR spectrometer and referenced to residual proton peaks of the deuterated solvent. Mass spectra were obtained by using an Agilent 1100 Series LC/MSD or a JEOL JMS-600W mass spectrometer. 2-(2,4-Difluorophenyl)pyridine (dfppy) and the chloride-bridged Ir(III) dimer ($[Ir(dfppy)_2(\mu\text{-}Cl)]_2$) were synthesized according to a literature method.[1,2] A fluorescent zinc sensor, Zinpyr-1 (ZP1), was prepared as reported previously.[3]

4-Formyl-1,10-phenanthroline. A modification of a literature procedure[4] was applied for this synthesis. 4-Methyl-1,10-phenanthroline (2.00 g, 10.3 mmol) and SeO_2 (2.45 g, 22.0 mmol) were suspended in 1,4-dioxane and H_2O (192 mL/8 mL), and the reaction mixture was refluxed for 2 h. After cooling, the solution was filtered through celite to remove black particulates. Concentration under vacuum and subsequent alumina (basic, EMD) column purification gave a white powder (0.541 g, 25%). ^{1}H NMR (MeOD, 400 MHz) δ: 7.70 (dd, J = 8.0, 4.4 Hz, 1H), 7.99 (d, J = 9.2 Hz, 1H), 8.01 (d, J = 4.4 Hz, 1H), 8.30 (dd, J = 8.0, 1.3 Hz, 1H), 9.03 (d, J = 9.2 Hz, 1H), 9.23 (dd, J = 4.4, 1.6 Hz, 1H), 9.47 (d, J = 4.4 Hz, 1H), 10.59 (s, 1H). ^{13}C NMR (MeOD, 100 MHz) δ: 122.33, 123.89, 125.04, 126.82, 128.58, 129.70, 136.13, 136.82, 145.75, 147.47, 150.62, 151.04, 192.94.

4-(Di(2-picolyl)aminomethyl)-1,10-phenanthroline. 4-Formyl-1,10-phenanthroline (0.762 g, 3.66 mmol) and di(2-picolyl)amine (0.729 g, 3.66 mmol) were dissolved in fresh MeOH (70 mL). A catalytic amount (two drops) of glacial acetic acid was added to the solution, which was refluxed for 0.5 h. The reaction mixture was cooled by using an ice bath, and then $NaBH_3CN$ (0.460 g, 7.32 mmol) was slowly delivered to the solution. The ice bath was removed and the reaction mixture was stirred overnight at room temperature. Basic work-up using saturated aqueous sodium carbonate solution and subsequent extraction using CH_2Cl_2 was performed. The organic layer was recovered, dried over anhydrous $MgSO_4$, and concentrated by vacuum. The crude product was subjected to silica gel column chromatography (CH_2Cl_2 to CH_2Cl_2:MeOH = 19:1, v/v), affording a sticky brown solid (0.892 g, 62%). ^{1}H NMR (MeOD, 400 MHz) δ: 3.71 (s, 4H), 4.03 (s, 2H), 6.92 (m, 2H), 7.23 (d, J = 8.0 Hz, 2H), 7.34 – 7.42 (m, 3H), 7.52 (d, J = 9.2 Hz, 1H), 7.61 (d, J = 4.4 Hz, 1H), 7.88 (d, J = 9.2 Hz, 1H), 7.98 (dd, J = 3.2, 1.6 Hz, 1H), 8.32 (m, 2H), 8.90 (d, J = 4.4 Hz, 1H), 8.93 (dd, J =

4.2, 1.6 Hz, 1H). ^{13}C NMR (MeOD, 100 MHz) δ: 55.63, 60.44, 122.16, 122.76, 122.86, 123.15, 123.52, 125.86, 127.67, 128.04, 135.67, 136.39, 144.69, 146.15, 146.27, 148.95, 149.76, 150.03, 158.62.

ZIrF. The chloride-bridged Ir(III) dimer, $[(dfppy)_2Ir(\mu\text{-}Cl)]_2$ (1.09 g, 0.894 mmol) and 4-(di(2-picolyl)aminomethyl)-1,10-phenanthroline (0.484 g, 0.664 mmol) were dissolved in anhydrous CH_2Cl_2 (30 mL) and the mixture was refluxed for 6 h. Color of the solution turned orange. At room temperature, NH_4PF_6 (15 equiv) was slowly added to the reaction mixture and the solution was stirred for additional 12 h. After removal of residual NH_4PF_6 by filtration, the crude product was concentrated under vacuum and purified by silica gel column chromatography (CH_2Cl_2 to CH_2Cl_2:MeOH = 9:1, v/v). Additional repeated purification steps on preparative TLC (silica) plates using 5 vol % MeOH in CH_2Cl_2 as a developing eluent afforded a yellow powder (0.226 g, 11%). ^{1}H NMR (MeOD, 400 MHz) δ: 3.96 (s, 4H), 4.46 (dd, J = 5.0, 1.6 Hz, 2H), 5.73 (m, 2H), 6.58 (m, 2H), 6.90 (m, 1H), 6.97 (m, 1H), 7.12 (broad m, 2H), 7.25 (d, J = 7.2 Hz, 1H), 7.31 (d, J = 6.0 Hz, 1H), 7.45 (d, J = 7.6 Hz, 2H), 7.63 (m, 2H), 7.71 (m, 2H), 7.82 (dd, J = 8.4, 5.2 Hz, 1H), 8.10 (m, 1H), 8.13 – 8.19 (m, 2H), 8.22 – 8.33 (m, 4H), 8.49 (m, 2H), 8.66 (d, J = 8.0 Hz, 2H). ^{13}C NMR (MeOD, 100 MHz) δ: 55.25, 60.67, 99.42, 99.49, 99.56, 114.22, 114.39, 122.94, 123.77, 124.01, 124.11, 125.23, 126.81, 127.05, 127.91, 128.81, 131.15, 131.72, 137.53, 139.32, 139.80, 146.31, 146.69, 149.00, 149.12, 149.19, 150.29, 150.42, 150.85, 153.57, 153.64, 153.68, 157.97, 160.32 (d, J = 13 Hz), 162.64 (d, J = 12 Hz), 162.92 (d, J = 13 Hz), 164.38, 164.40, 164.42, 165.21 (d, J = 13 Hz). ^{19}F NMR (MeOD, 376 MHz) δ: −108.77 (m, 2F), −105.74 (m, 2F), −73.23 (d, J = 768 Hz, 6F). ^{31}P NMR (MeOD, 161 MHz) δ: −144.09 (sept, J = 714 Hz). HRMS (ESI, positive): $[M\text{-}PF_6^-]^+$ calcd for $C_{47}H_{33}F_4IrN_7$, 964.2363; found, 964.2363. Anal. Calcd for $C_{47}H_{33}F_{10}IrN_7P$: C, 50.90; H, 3.00; N, 8.84. Found: C, 50.81; H, 3.01; N, 8.84.

IrF. IrF was synthesized by an identical method used for ZIrF using 0.500 g (0.411 mmol) of the chloride-bridged Ir(III) dimer, $[(dfppy)_2Ir(\mu\text{-}Cl)]_2$ and 0.148 g (0.822 mmol) of 1,10-phenanthroline. Isolated product was yellow powder (0.497 g, 67%). ^{1}H NMR (MeOD, 400 MHz) δ: 5.93 (dd, J = 8.6, 2.4 Hz, 2H), 6.78 (m, 2H), 7.07 (t, J = 6.0 Hz, 2H), 7.77 (d, J = 5.2 Hz, 2H), 7.98 (t, J = 8.4 Hz, 2H), 8.10 (dd, J = 8.2, 4.8 Hz, 2H), 8.38 (d, J = 8.4 Hz, 2H), 8.43 (s, 2H), 8.59 (dd, J = 5.2, 1.2 Hz, 2H), 8.94 (dd, J = 8.0, 1.2 Hz, 2H). ^{13}C NMR (MeOD, 100 MHz) δ: 98.74, 98.81, 98.88, 113.94, 114.04, 123.50, 123.60, 124.07, 127.27, 128.60, 131.92, 139.48, 139.62, 146.61, 149.96, 151.69, 154.09, 154.13, 160.12 (d, J = 12 Hz), 162.31 (d, J = 13 Hz), 162.71 (d, J = 13 Hz), 163.87, 163.91, 164.83 (d, J = 13 Hz), 164.87. ^{31}P NMR (MeOD, 161 MHz) δ: −143.53 (sept, J = 641 Hz). MS (ESI, positive): $[M]^+$ calcd for $C_{34}H_{20}F_4IrN_4$, 753.1; found, 752.9.

Femtosecond Laser Flash Photolysis. Femtosecond transient absorption spectroscopy experiments were conducted using an ultrafast source, Integra-C (Quantronix Corp.), an optical parametric amplifier, TOPAS (Light Conversion Ltd.), and a commercially available optical detection system, Helios provided by Ultrafast Systems LLC. The source for the pump and probe pulses was derived from the fundamental output of Integra-C (780 nm, 2 mJ/pulse and fwhm = 130 fs) at a repetition rate of 1 kHz. A 75% portion of the fundamental output of the laser was introduced into TOPAS, which has optical frequency mixers resulting in a tunable range from 285 nm to 1660 nm, while the rest of the output was used to generate white light. Prior to generating the probe continuum, a variable neutral density filter was inserted in the path in order to obtain a stable continuum, then the laser pulse was fed to a delay line that provides an experimental time window of 3.2 ns with a maximum step resolution of 7 fs. An excitation wavelength at 420 nm of TOPAS output, the fourth harmonic of signal or idler pulses, was chosen as the pump beam. Because this TOPAS output consists of not only the desired wavelength but also unnecessary wavelengths, the latter were deflected by using a wedge prism with a wedge angle of 18°. The desired beam was used to irradiate the sample cell with a spot size of 1 mm diameter where it merged with the white probe pulse at a small angle (< 10°). The probe beam, after passing through the 2 mm sample cell, was focused on a fiber optic cable, which was connected to a CCD spectrograph for recording the time-resolved spectra (470 – 1300 nm). Typically, 3000 excitation pulses were averaged for 3 s to obtain the transient spectrum at a set delay time. Kinetic traces at appropriate wavelengths were assembled from the time-resolved spectral data. All measurements were conducted at room temperature, 295 K.

Determination of Singlet Oxygen Generation Quantum Yields. The quantum yield for photosensitized singlet oxygen generation ($\Phi(^1O_2)$) was determined according to a literature procedure.[5] Air-equilibrated DMSO solutions containing a singlet oxygen sensitizer and a substrate (10 μM), 1,3-diphenylisobenzofuran (DPBF), were photoexcited with a hand-held UV lamp (10 mW, 365 nm). The absorbance of DPBF at 418 nm was recorded every 6 s. The O.D. of ZIrF was 0.20. Methylene blue (O.D. = 0.17) was employed as a reference for singlet oxygen sensitization ($\Phi(^1O_2)$ = 0.52). A DMSO solution of DPBF without a singlet oxygen sensitizer was examined to assess its photostability under identical irradiation conditions. Eq S1 was employed for the determination of $\Phi(^1O_2)$. In eq S1, m is the slope of a linear fit to data shown in Figure S12d and $F = 1-10^{-O.D.}$, where O.D. refers to the optical density of ZIrF or MB at 365 nm.

$$\Phi(^1O_2) = \Phi_{ref}(^1O_2) \times \frac{m \cdot F_{ref}}{m_{ref} \cdot F} \quad \text{(S1)}$$

Mathematical derivations of eqs 2 and 3

1) Equilibria

$Ir + H \rightleftharpoons IrH$; $K_a = [Ir][H]/[IrH]$

$Ir + Zn \rightleftharpoons IrZn$; $K_d = [Ir][Zn]_{free}/[IrZn]$

2) Relationships

(1) Total phosphorescence intensity (*P.I.*)

$P.I. = \alpha_1[Ir] + \alpha_2[IrH] + \alpha_3[IrZn]$

(2) Total concentration of ZIrF ($[Ir]_{total}$)

$[Ir]_{total} = [Ir] + [IrH] + [IrZn]$

(3) Total concentration of zinc ($[Zn]_{total}$)

$[Zn]_{total} = [Zn]_{free} + [IrZn]$

3) Rearrangement of above equations affords equation 3 and 4 at pH 7.0

$$P.I. = \{(\alpha_1 + 0.00263\alpha_2 + \alpha_3[Zn]_{free}/K_d)/(1.00263 + [Zn]_{free}/K_d)\} \times [Ir]_{total} \quad (3)$$

$$[Zn]_{free}^2 + ([Ir]_{total} - [Zn]_{total} + 1.00263K_d)[Zn]_{free} - 1.00263K_d[Zn]_{total} = 0 \quad (4)$$

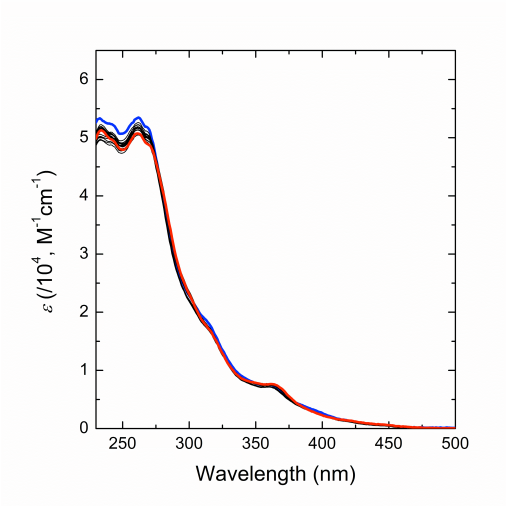

Figure S1. UV-vis absorption spectra of ZIrF (10 μM, CH_3CN) with increasing concentration of $Zn(ClO_4)_2$ (0 – 1.8 equiv). Blue and red lines are absorption spectra in the absence and presence (1.8 equiv) of zinc, respectively.

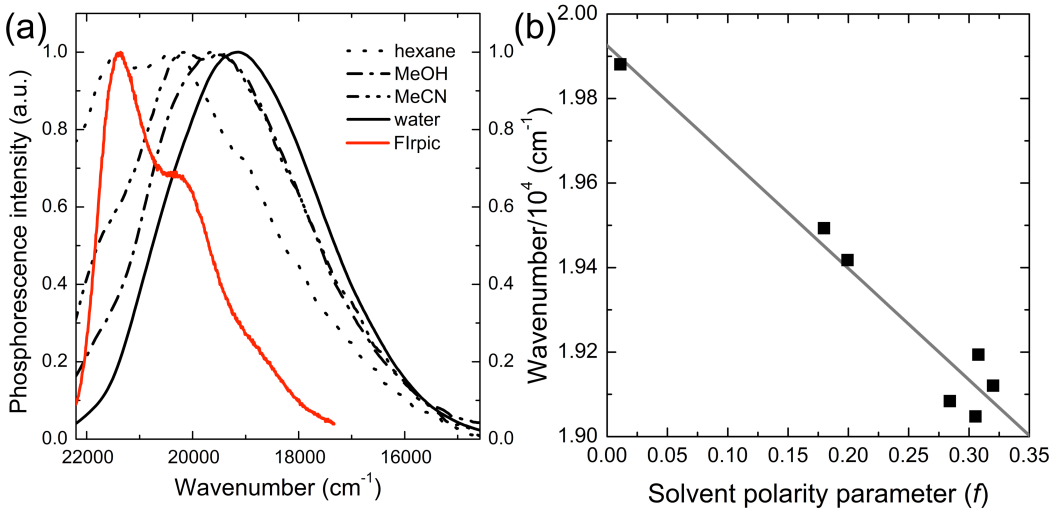

Figure S2. Solvatochromism of ZIrF. (a) Phosphorescence spectra in solvents of different polarity. (b) Lippert-Mataga plot displaying peak emission wavelength as a function of solvent polarity parameter (f = $(\varepsilon-1)/(2\varepsilon+1)$ $-(n^2-1)/(2n^2+1)$; ε and n are dielectric constant and refractive index of solvent, respectively). Air-equilibrated ZIrF solutions (10 μM) were excited at 340 nm. The phosphorescence spectrum of FIrpic[6] (10 μM, CH_3CN) having identical cyclometalating ligands of ZIrF and a non-chromophoric acetylacetonato ligand is included for comparison (red solid line).

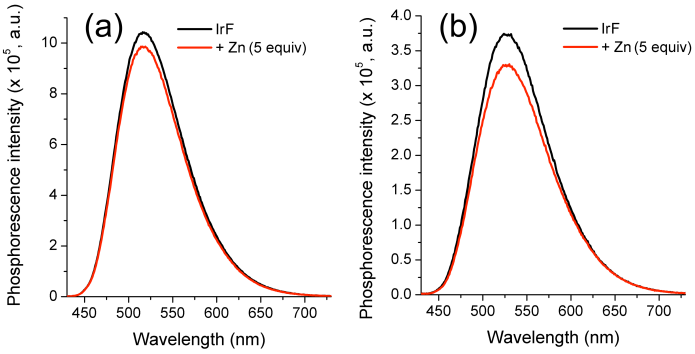

Figure S3. Change in phosphorescence spectrum of IrF (10 μM) in response to zinc ion. (a) CH_3CN and (b) pH 7.0 buffer (25 mM PIPES) solutions. λ_{ex} = 340 nm.

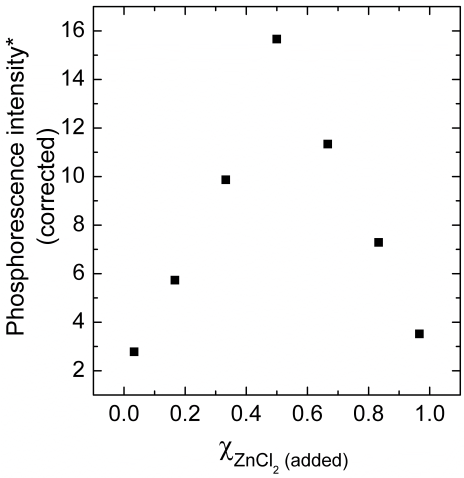

Figure S4. Phosphorescence Job's plot of ZIrF with varying mole fractions of zinc ion. Total salt concentration was kept to 10 μM. pH 7.0 buffer (25 mM PIPES) was used for the measurement. λ_{ex} = 340 nm.

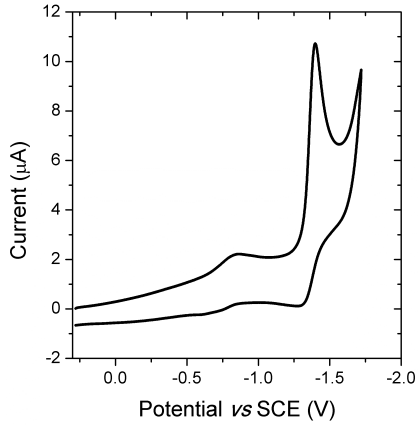

Figure S5. Cyclic voltammogram of the reduction sweep for ZIrF. Conditions: Scan rate = 100 mV/s; 1 mM in an Ar-saturated acetonitrile containing Bu_4NPF_6 (0.1 M) supporting electrolyte. Pt wires were used as the counter and working electrodes. The $Ag/AgNO_3$ couple was the reference electrode.

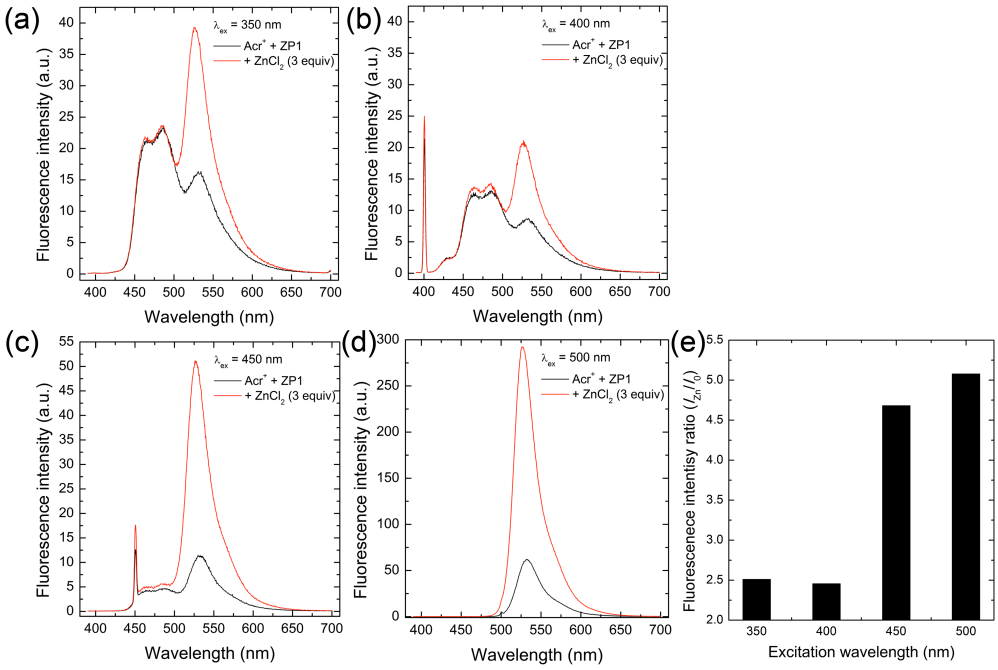

Figure S6. Fluorescence spectra of pH 7.0 buffer solutions (25 mM PIPES) containing ZP1 (5 μM) and Acr^+ (50 μM) in the absence and presence of $ZnCl_2$ (3 equiv) at excitation wavelength = 350 nm (a), 400 nm (b), 450 nm (c), and 500 nm. (d) Corresponding fluorescence intensity ratios (I_{Zn}/I_0).

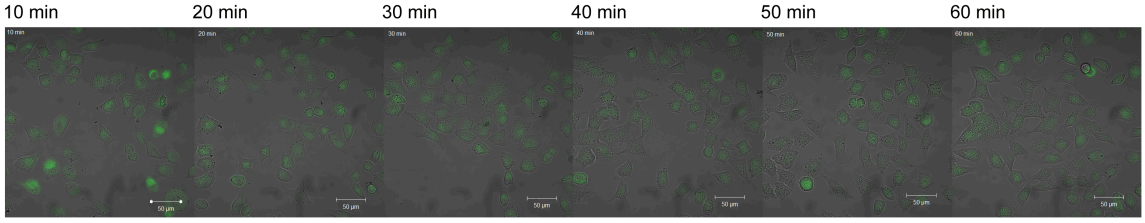

Figure S7. Phosphorescence microscope images of live A549 cells incubated with ZIrF. Images were taken for treated cells at different incubation times of 10 – 60 min.

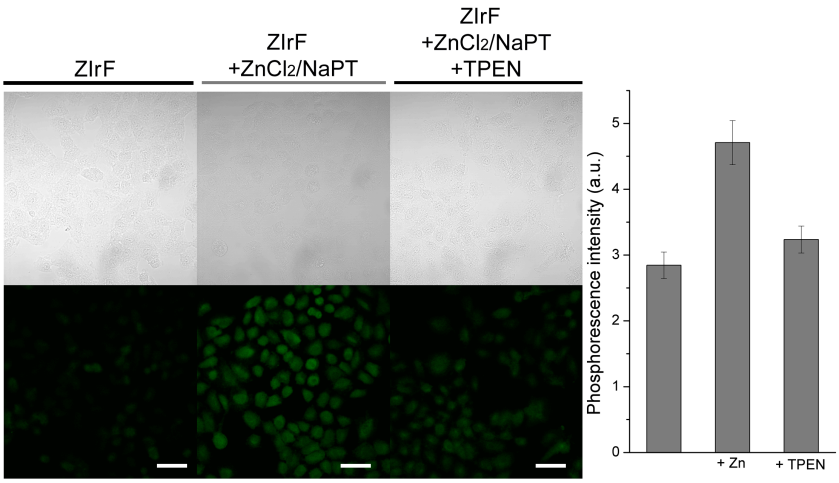

Figure S8. Phosphorescent imaging of intracellular zinc ions of fixed A549 cells. Shown at the right are corresponding phosphorescence intensities from the processed images.

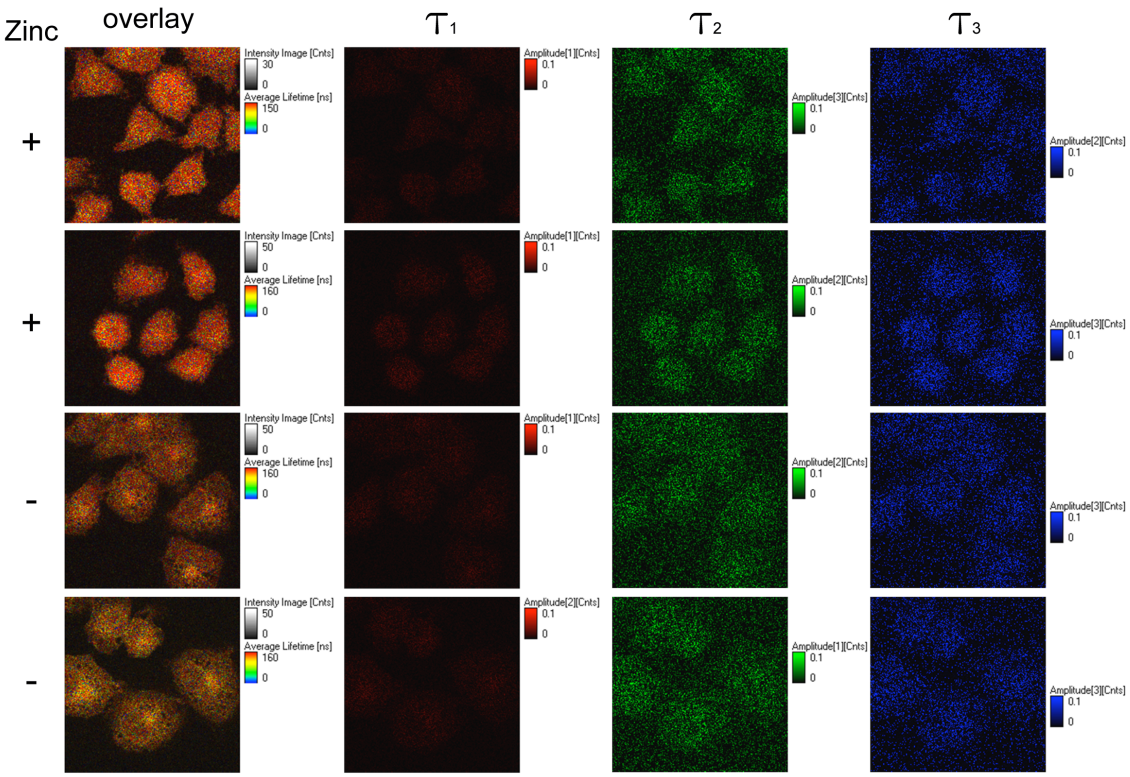

Figure S9. Fluorescence lifetime imaging of fixed A549 cells treated with ZIrF.

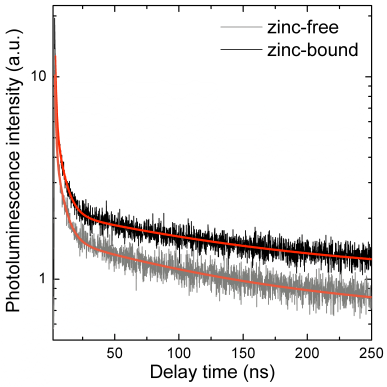

Figure S10. Averaged decay profiles of photoluminescence lifetime images shown in Figure 12 in the main text. Black and grey lines are decay traces of zinc-supplemented A549 cells and untreated A549 cells, respectively. Red and orange solid curves are triple exponential fits of the respective decay traces. Refer to Table 3 for fit results.

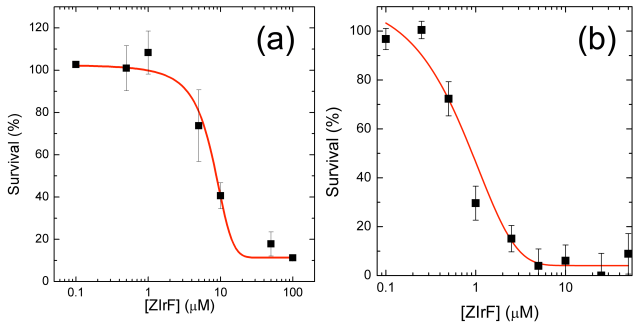

Figure S11. MTT cell viability assays for (a) A549 (5 h, 37 °C) and (b) HeLa cells (12 h, 37 °C) treated with ZIrF.

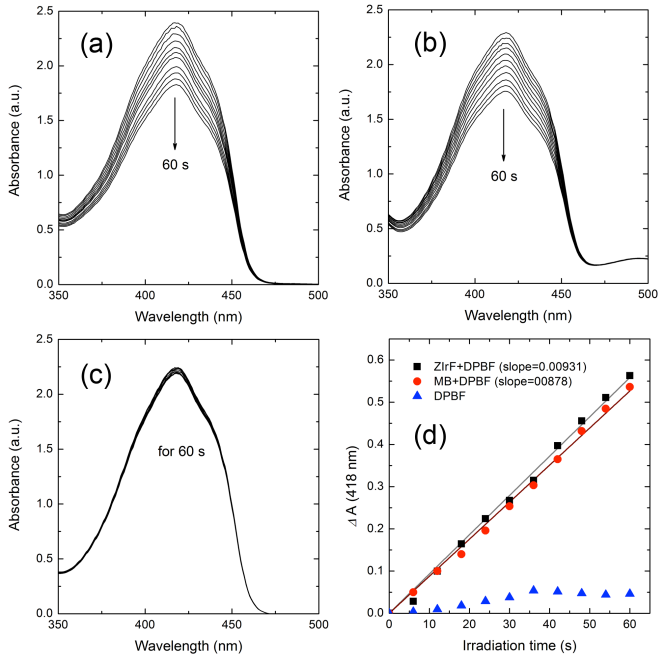

Figure S12. Singlet oxygen generation in the presence of (a) ZIrF and (b) methylene blue (MB; reference compounds, $\Phi(^1O_2)$ = 0.52). DMSO solutions containing either ZIrF or MB and 1,3-diphenylisobenzofuran (DPBF) as an oxidation substrate were irradiated under UV light (365 nm). (c) DMSO solution of DPBF without a singlet oxygen generating sensitizer was used as a control. (d) Changes were monitored in the 418 nm absorption band of DPBF as a function of irradiation time. Singlet oxygen quantum yields ($\Phi(^1O_2)$) were calculated by the equation S1, in which *m* is the slope of a linear fit to data shown in Figure S12d and $F = 1-10^{-O.D.}$, where O.D. refers to the optical density of ZIrF or MB at 365 nm. Refer to Experimental details in p. S4.

$$\Phi(^1O_2) = \Phi_{ref}(^1O_2) \times \frac{m \cdot F_{ref}}{m_{ref} \cdot F} \qquad (S1)$$

Table S1. Selected Metric Parameters for the Calculated Structures of ZIrF and IrF

entry	distance (Å)			angle (°)	
	Ir–N_{phen}	Ir–N_{dfppy}	Ir–C_{dfppy}	N–Ir–C	N–Ir–N
ZIrF	2.206	2.079	2.019	80.1	75.8
IrF	2.210	2.081	2.018	80.1	75.9

Table S2. Analysis of the Decay Traces of the FLIM Images Shown in Figure S9

zinc	τ_{avg} (ns)	A_1	τ_1 (ns)	A_2	τ_2 (ns)	A_3	τ_3 (ns)	χ^2
+	130	87	150	240	6.8	530	0.98	0.99(5)
+	135	81	160	180	9.0	540	1.6	1.0(3)
−	130	99	150	260	7.2	580	0.94	0.99(2)
−	120	93	140	280	6.1	580	0.78	0.97(3)

References

(1) Nonoyama, M. *Bull. Chem. Soc. Jpn.* **1974**, *47*, 767-768.

(2) Tamayo, A. B.; Alleyne, B. D.; Djurovich, P. I.; Lamansky, S.; Tsyba, I.; Ho, N. N.; Bau, R.; Thompson, M. E. *J. Am. Chem. Soc.* **2003**, *125*, 7377−7387.

(3) Burdette, S. C.; Walkup, G. K.; Spingler, B.; Tsien, R. Y.; Lippard, S. J. *J. Am. Chem. Soc.* **2001**, *123*, 7831-7841.

(4) Zaid, A.; Sun, J.-S.; Nguyen, C.-H.; Bisagni, E.; Garestier, T.; Grierson, D. S.; Zain, R. *ChemBioChem* **2004**, *5*, 1550-1557.

(5) Adarsh, N.; Avirah, R. R.; Ramaiah, D. *Org. Lett.* **2010**, *12*, 5720–5723.

(6) Holmes, R. J.; Forrest, S. R.; Tung, Y.-J.; Kwong, R. C.; Brown, J. J.; Garon, S.; Thompson, M. E. *Appl. Phys. Lett*. **2003**, *82*, 2422–2424.

Complete Citation of Reference 123

(123) Frisch, M. J.; Trucks, G. W.; Schlegel, H. B.; Scuseria, G. E.; Robb, M. A.; Cheeseman, J. R.; Montgomery, J. A. J.; Vreven, T.; Kudin, K. N.; Burant, J. C.; Millam, J. M.; Iyengar, S. S.;

Tomasi, J.; Barone, V.; Mennucci, B.; Cossi, M.; Scalmani, G.; Rega, N.; Petersson, G. A.; Nakatsuji, H.; Hada, M.; Ehara, M.; Toyota, K.; Fukuda, R.; Hasegawa, J.; Ishida, M.; Nakajima, T.; Honda, Y.; Kitao, O.; Nakai, H.; Klene, M.; Li, X.; Knox, J. E.; Hratchian, H. P.; Cross, J. B.; Bakken, V.; Adamo, C.; Jaramillo, J.; Gomperts, R.; Stratmann, R. E.; Yazyev, O.; Austin, A. J.; Cammi, R.; Pomelli, C.; Ochterski, J. W.; Ayala, P. Y.; Morokuma, K.; Voth, G. A.; Salvador, P.; Dannenberg, J. J.; Zakrzewski, V. G.; Dapprich, S.; Daniels, A. D.; Strain, M. C.; Farkas, O.; Malick, D. K.; Rabuck, A. D.; Raghavachari, K.; Foresman, J. B.; Ortiz, J. V.; Cui, Q.; Baboul, A. G.; Clifford, S.; Cioslowski, J.; Stefanov, B. B.; Liu, G.; Liashenko, A.; Piskorz, P.; Komaromi, I.; Martin, R. L.; Fox, D. J.; Keith, T.; Al-Laham, M. A.; Peng, C. Y.; Nanayakkara, A.; Challacombe, M.; Gill, P. M. W.; Johnson, B.; Chen, W.; Wong, M. W.; Gonzalez, C.; Pople, J. A.; Gaussian 03 Revision D.01 ed.; Gaussian, Inc.,: Wallingford CT, 2004.